arXiv:1405.2723v1 [cond-mat.quant-gas] 12 May 2014

Isospin Correlations in two-partite Hexagonal Optical Lattices

Marta Prada,[1,*] Eva-Maria Richter,[1,*] and Daniela Pfannkuche[1]

[1] *I. Institut für Theoretische Physik, Universität Hamburg, Jungiusstr. 9, 20355 Hamburg, Germany*

Two-component mixtures in optical lattices reveal a rich variety of different phases. We employ an exact diagonalization method to obtain the relevant correlation functions in hexagonal optical lattices to characterize those phases. We relate the occupation difference of the two species to the magnetic polarization. 'Iso'-magnetic correlations disclose the nature of the system, which can be of easy-axis type, bearing phase segregation, or of easy-plane type, corresponding to super-counter-fluidity. In the latter case, the correlations reveal easy-plane segregation, involving a highly-entangled state. We identify striking correlated supersolid phases appearing within the superfluid limit.

I. INTRODUCTION

Ultracold quantum gases in optical lattices have long been recognized as a field of growing interest owing to the possibility to prepare, manipulate and control a quantum system, hence *quantum engineering* [1–6]. The idealities in optical lattices have indeed been extensively employed as quantum simulators for many-body physics [7–13]. Multicomponent systems provide, for example, an ideal platform on which to study magnetic ordering [14, 15]. In particular, multicomponent graphene-like structures are boasting a profound impact in condensed-matter physics owing not only to the fascinating properties of graphene itself, but also to the rich quantum phases they exhibit [16–21].

In this work we explore the extended phase diagram of a two-component hexagonal optical lattice. Most of the theoretical studies employ approximate methods to describe the Mott-insulator regime [14, 22–27], or perform expansions around the superfluid regime [28]. On the contrary, we address in the present work the phase diagram on its full range, from weak to strong coupling, by employing an exact diagonalization method. We aim for the iso-magnetic correlations beyond the weak coupling limits, and explore in particular the superfluid regime. Such technique is of particular significance, since quantum correlations are central to understanding spin ordering and non-local string ordering [29]. We identify ferro- and anti-ferromagnetic correlated regimes, where we find striking supersolid [30–33] and highly-entangled super-counter-fluid (SCF) phases [22, 34, 35], respectively.

II. METHODS

Our numerical simulations are based on the single band Bose-Hubbard-Model [2] for a two component Bose mixture (boson 'A' and boson 'B') with nearest neighbor (NN) hopping, which we describe by a Hubbard Hamiltonian,

$$H = H_{\rm o} + H_{\rm hop}, \tag{1}$$

$$H_{\rm o} = \sum_i \left\{ \frac{U}{2}\left[\hat{n}_A^i(\hat{n}_A^i-1)+\hat{n}_B^i(\hat{n}_B^i-1)\right] + V\hat{n}_A^i\hat{n}_B^i \right\}, \tag{2}$$

$$H_{\rm hop} = -t\sum_{\langle ij\rangle_1}\left(\hat{a}_i^\dagger\hat{a}_j+\hat{b}_i^\dagger\hat{b}_j+{\rm c.c.}\right). \tag{3}$$

Here, i runs over the N sites of our unit cell, t describes the hopping for both species, U, V are the on-site repulsion for equal and different species, respectively, $\hat{a}$, $\hat{a}^\dagger$ ($\hat{b}$, $\hat{b}^\dagger$) are the annihilation and creation operators, respectively, for the A (B) particle, and $\hat{n}_{\rm A} = \hat{a}^\dagger\hat{a}$ ($\hat{n}_{\rm B} = \hat{b}^\dagger\hat{b}$) the particle number operators. $\langle ij\rangle_1$ indicates that the sum is performed over first NN. The Hamiltonian of Eq. (3) suggest expressing the Hilbert space in terms of occupation numbers, being spanned by all possible configurations of a fixed N and fixed fillings $\langle n_\alpha^i\rangle$ = 1/2, α = A, B, yielding the holonomic constraint $\langle\hat{n}_{\rm A}^i+\hat{n}_{\rm B}^i\rangle = 2S$, with $S = 1/2$. We evaluate all observables in the ground state of (1), $|\psi_{\rm GS}\rangle$, which we calculate employing an exact diagonalization method (Lanczos algorithm) with periodic boundary conditions. Throughout this work, we employ the notation $\langle{\rm O}\rangle \equiv \langle\psi_{\rm GS}|{\rm O}|\psi_{\rm GS}\rangle$.

The on-site term can be expressed, omitting trivial constant terms, as

$$H_{\rm o} = U\left[(\hat{S}_x^i)^2+(\hat{S}_y^i)^2+2(\hat{S}_z^i)^2\right]+V\left[(\hat{S}_x^i)^2+(\hat{S}_y^i)^2\right], \tag{4}$$

where we have employed the iso-spin, $\hat{S}_z^i = (\hat{n}_{\rm A}^i-\hat{n}_{\rm B}^i)/2$, within the Schwinger boson representation [36]: $\hat{S}_\pm^i = \hat{S}_x^i \pm i\hat{S}_y^i$, with $\hat{S}_+^i = \hat{a}_i^\dagger\hat{b}_i$ and $\hat{S}_-^i = \hat{b}_i^\dagger\hat{a}_i$. In view of Eq. (4), a first approach to understanding the magnetic phases is by evaluating the on-site square of the spin components, $\langle\hat{S}_z^2\rangle \equiv \sum_i\langle(\hat{S}_z^i)^2\rangle/N$ and $\langle\hat{S}_\parallel^2\rangle \equiv \sum_i[\langle(\hat{S}_x^i)^2+(\hat{S}_y^i)^2\rangle]/N$, allowing to classify the ground state as easy-plane or easy-axis type.

It is customary to distinguish between the weak coupling, low mobility limit, also termed as 'Mott insulator' (MI) and a high-mobility, or superfluid regime (SF). The SF is thus characterized by a wavefunction broaden over the entire lattice, as opposed to localized at the lattice sites, which occurs in the MI regime. Both limits can be distinguished by the mean particle fluctuations,

$$\langle\Delta\hat{n}\rangle = \sqrt{\langle(\hat{n}_{\rm A}+\hat{n}_{\rm B})^2\rangle-\langle\hat{n}_{\rm A}+\hat{n}_{\rm B}\rangle^2} = \sqrt{4\langle\hat{S}^2\rangle-3}. \tag{5}$$

* These two authors contributed equally

Naturally, $\Delta\hat{n}$ is expected to be small (large) in the MI (SF) regime. We stress that our exact diagonalization method is not limited to the MI regime in this work, but rather we explore the entire parametric region. We also note that in the superfluid phase, the usual restriction to spin $S = 1/2$ states per site can not be applied in the SF regime.

It is well known that in the weak coupling, MI limit, $t < V,U$ the hopping term of Eq. (3) can be mapped onto an effective iso-spin Hamiltonian by a Schrieffer-Wolff-transformation [22, 23], resulting in the anisotropic Heisenberg spin-1/2 model,

$$H_{\rm hop} = \frac{t^2}{2}\left(\frac{1}{U}-\frac{1}{V}\right)\left(\hat{S}^i_-\hat{S}^j_+ + \hat{S}^i_+\hat{S}^j_- - \hat{S}^i_z\hat{S}^j_z\right). \qquad (6)$$

However, we are also interested in the SF limit, where finite multiple occupation makes the mapping complicated to visualize. To explore the magnetic ordering in any regime, we introduce the easy-axis pair-correlation function,

$$g^z_{ij} = \langle \hat{n}^i_{\rm A}\hat{n}^j_{\rm A} + \hat{n}^i_{\rm B}\hat{n}^j_{\rm B} - \hat{n}^i_{\rm A}\hat{n}^j_{\rm B} - \hat{n}^i_{\rm B}\hat{n}^j_{\rm A}\rangle.$$

The first two terms can be identified with ferromagnetic (FM) contributions and the last two, with anti-ferromagnetic (AFM) ones. $g^z_{ij} = {\rm FM} - {\rm AFM}$, is thus an observable that quantifies the magnetic ordering, being (anti)-ferromagnetic when positive (negative). In view of Eq. (6), we expect a FM order in the limit $V > U \gg t$, since the prefactor of $\hat{S}^i_z\hat{S}^j_z$ is positive. Likewise, one may expect AFM ordering in the $U > V \gg t$, where the prefactor changes sign. As we will see below, however, in the SF limit $U,V \gtrsim t$ entanglement plays a key role in determining the nature of the quantum magnetic phases in the SF limit, which are far from being obvious.

Entangled states suggest the exploration of pair-correlation functions also within the easy-plane,

$$g^{\parallel}_{ij} \equiv \langle \hat{\vec{S}}^i_{\parallel}\hat{\vec{S}}^j_{\parallel}\rangle = \langle \hat{S}^i_+\hat{S}^j_- + \hat{S}^i_-\hat{S}^j_+\rangle,$$

with $g^{\parallel}_{ij}$ being an observable that quantifies the entanglement between sites 'i' and 'j'. The different correlation functions reveal indeed a rich phase diagram, as will be seen in the next section.

III. RESULTS

We choose a unit cell larger than the customary hexagonal lattice's unit cell for our numerical calculations, since the hopping term breaks translational symmetry, which is only restored on a mean field level. We first consider the unit cell depicted in the insets of Fig. 1(a) (broken lines), with $N = 8$, commensurate with a super-solid phase (see below). The next unit cell in size commensurate with the super-solid while preserving the D_6 point group symmetry of the lattice contains 24 sites, which is beyond the limit of our present computational capabilities.

To investigate the magnetic character, we first calculate the square of the on-site out-of-plane (easy axis) and in-plane (easy plane) components of spin, $\langle \hat{S}^2_z\rangle$ and $\langle \hat{S}^2_{\parallel}\rangle$. The out-of-plane component is largest in the $V > U$ region, as shown in Fig. 1(a): the dark blue colored region, $\langle \hat{S}^2_z\rangle > 1/4$, reflects multiple occupation of single sites with alike particles. On the contrary, Fig. 1(b) demonstrates an easy-plane ground state in the region $V \lesssim 10t$, revealing entanglement of bosons of different species rather than just the alternating arrangement of the right inset of Fig. 1(a). Easy-plane state implies super counter-flow (SCF) states [22, 27, 34]. We stress that the square of the total spin per site is only a 'good' quantum number in the limit $U,V \gg t$, where $\langle \hat{S}^2\rangle = 3/4$ [dark-blue in Fig. 2(a)]. The insets of Fig. 1(a) illustrate the MI FM and AFM

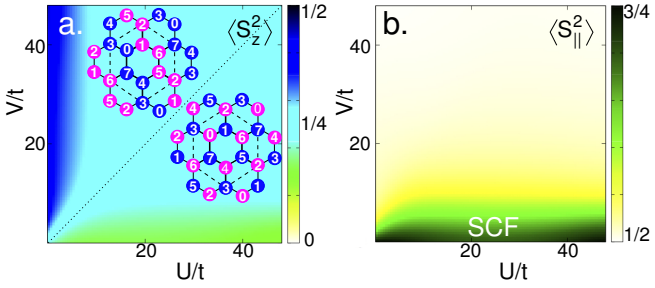

Figure 1. Numerical results for the on-site square of the spin components, easy-axis (a) and easy-plane (b). Insets of (a) depicts the FM ($V > U$) and AFM ($U > V$) phase, with the broken lines marking the unit cell boundaries.

phases occurring at $V > U$ and $U > V$, respectively. Blue and magenta circles encode the two bosonic species, 'A' and 'B'.

We now evaluate the averaged particle fluctuations $\Delta\hat{n}$ defined in Eq. (5). The results are presented in Fig. 2 (a) as a function of on-site interaction parameters, V and U. The MI regime (dark blue region) is characterized by low particle fluctuations, with the bosons being localized at the lattice sites and hence, well defined $\langle \hat{S}^2\rangle = 3/4$. On the contrary, in the SF regime (rainbow colored region), the fluctuations imply $\Delta n > 0$ (or $\langle \hat{S}^2\rangle > 3/4$). The dashed black curve of Fig. 2(a)

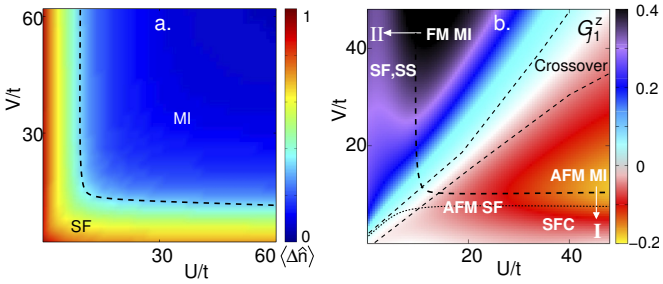

Figure 2. (a) Numerical results for the particle fluctuation $\langle\Delta\hat{n}\rangle$ as a function of the on-site interactions, U and V. A low mobility, MI phase (dark blue) and a high-mobility, SF phase (red to cyan) are apparent. The dashed line defines the boundary between both limits (arbitrary). (b) Numerical results of $\mathcal{G}^z_1$ as a function of U and V. The sign of $\mathcal{G}^z_1$ determines the magnetic phases: FM (cyan-blue-purple-black) and AFM (red-yellow).

distinguishes the Mott-insulator and the superfluid phases. We stress that we do not attempt to determine a sharp, well defined

boundary between the different phases throughout this work, but rather to determine the overall ordering and magnetic character, by evaluating exact ground states of a finite size system. Sharp, well defined phase boundaries are expected to occur for certain order parameters in larger systems, for which we are computationally limited.

We next study the magnetic phases by computing the normalized easy-axis pair-density correlation function for NN,

$$\mathcal{G}_1^z = \sum_{\langle ij\rangle_1} \tilde{g}_{ij}^z = \frac{2n-1}{2} \sum_{\langle ij\rangle_1,\alpha\neq\beta} \left[\frac{\langle \hat{n}_\alpha^i \hat{n}_\alpha^j \rangle}{n-1} - \frac{\langle \hat{n}_\alpha^i \hat{n}_\beta^j \rangle}{n} \right], \quad (7)$$

where $\tilde{g}_{ij}^z$ is similar to g_{ij}^z, except for correcting factors to take into account finite size unit cells [40]. Fig. 2(b) shows the numerical results for $\mathcal{G}_1^z$ (color scale) as a function of U and V. The sign of $\mathcal{G}_1^z$ discriminates between FM ordering, when positive (blue-purple-black), and AFM ordering, when negative (red-yellow). In FM ordering (U<V), 'A' and 'B' bosons are mainly located in separated domains, whereas in AFM ordering (U>V) the bosons are in an entangled state rather than just alternating ordering. As a consequence, the absolute value of the magnetic ordering is larger in the FM region than in the AFM one [see Fig 1(b)]. At the crossover region $U \simeq V$, the ferro- and anti-ferromagnetic correlations have the same magnitude, owing to the inherent SU(2) symmetry (white), with 'A' and 'B' bosons being close to indistinguishable. Fig. 2 (b) reveals a region of large FM correlations (black) and a region of large AFM correlations (yellow), both shifted from the vertical ($U = 0$) and horizontal ($V = 0$) axis, respectively. These 'shifts' [see arrows in Fig. 3(a)] imply that (I) lowering U at constant V (increasing the V/U ratio), the FM character of the system decreases and (II) lowering V at constant U (increasing the U/V ratio), the AFM character decreases, both being in principle counterintuitive. These anomalies in $\mathcal{G}_1^z$ suggest exploring second and third NN correlations, $\mathcal{G}_{2(3)}^z$, as well as the analogous 'in-plane' correlations, $\mathcal{G}_n^{\parallel}$, defined as

$$\mathcal{G}_n^{\parallel} = \frac{1}{\Omega_n} \sum_{\langle ij\rangle_n} \langle \hat{S}_+^i \hat{S}_-^j + \hat{S}_-^i \hat{S}_+^j \rangle,$$

with Ω_n being the normalization factors, $\Omega_n = \eta_n(n_A + n_B)/2$, with η_n being the number of n-th NN, and the sum being performed for n-th NN.

Fig. 3 shows the numerical results for the easy-axis (a-c) and easy-plane (d-e) correlations for 1st (a, d), 2nd (b, e) and 3rd (c, f) NN. $\mathcal{G}_1^z$ is replotted here for clarity and completeness. It is worth noting the different color scales used to plot Fig. 3 (a-c), to enhance the relevant features. We first focus on the phase at 'I' [lower right of Fig. 3(a)]. The feature is reproduced in $\mathcal{G}_2^z$ [Fig. 3 (b)]. In the MI limit, alternating ordering enhances the out of plane correlations, which naturally are FM to second NN. Recalling the results of Fig. 1(b), we conclude that the spin lies mostly in the easy-plane at this region, bearing the reduction on $\mathcal{G}_{1,2}^z$ at phase 'I' with respect to the deep MI AFM phase. Multiple occupation in this phase within the SF regime is limited to two particles of different species (a third particle would be penalized, as it would imply

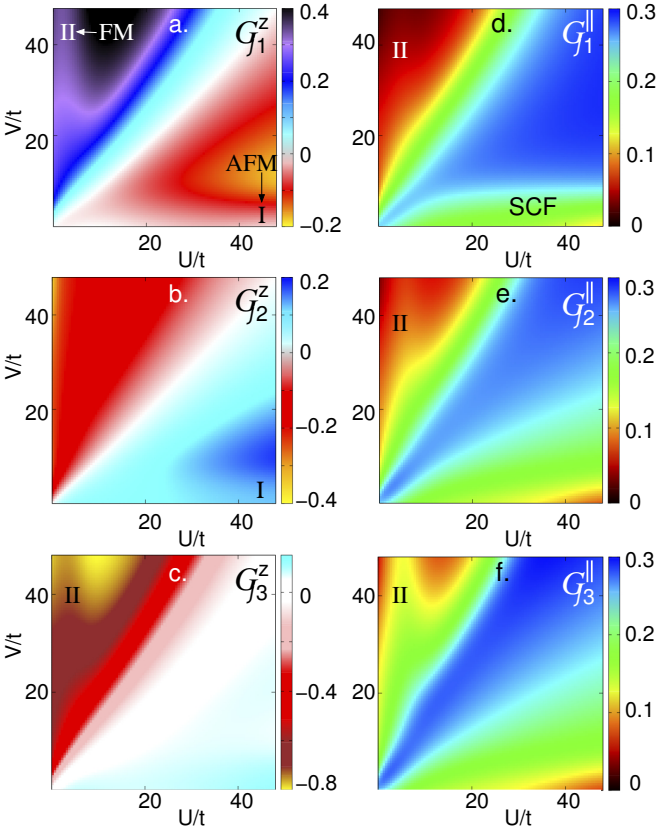

Figure 3. Numerical results for easy-axis (a-c) (note the different color scales) and easy-plane (d-e) correlation functions for first (a, d), second (b, e) and third (c, f) NN, for a unit cell with 8 sites.

two particles of same kind), implying doubly-occupied sites alternating with empty ones. This is reflected in the reduction of the in-plane correlations with respect to the AFM phase [lower right of Fig. 3 (d)]. We conclude that phase 'I' corresponds to a easy-plane state with in-plane FM ordering.

We now focus on the phase marked 'II' [upper left of Fig. 3(a)]. The feature is reproduced in $\mathcal{G}_3^z$ [see Fig. 3(c)]. It is worth noting that $\mathcal{G}_3^z$ indicates AFM character where $\mathcal{G}_1^z$ is FM, which is due to the finite size of the unitary cell. In the $V \gg U$ and within the SF regime, multiple-occupied states of same bosonic species would be expected, separated by the maximum distance d = 3 (recall that the unit cell has eight atoms). However, $\mathcal{G}_n^{\parallel}$ reveals a more complex situation [upper left of Fig. 3(d–f)], with the easy plane correlation functions peaking around this 'anomalous' region. For clarity, we present in Fig. 4(a) the $V/t = 50$ resuts for $\mathcal{G}_n^{\parallel}$, where the enhancemnets of the correlation functions are apparent. We identify the phase at 'II' with the formation of a super-solid, where a density wave of multiple occupied states alternate with entangled states, hence with a larger unit cell (see inset of Fig. 4b).

To demonstrate the formation of a super-solid phase, we

further explore higher order correlation functions, as:

$$\kappa_n = \frac{1}{\Omega_n} \sum_{\langle ij \rangle_n} \langle \hat{n}^i_{\rm A}(\hat{n}^i_{\rm A} - 1)(\hat{S}^i_- \hat{S}^j_+ + \hat{S}^i_+ \hat{S}^j_-) \rangle,$$

which can be viewed as a 'flip-flop' involving a triple-occupied site with at least two bosons of the same species. The correlation function κ_n for first ($n = 1$, red), second ($n = 2$, green) and third ($n = 3$, blue) NN is plotted in Fig. 4 (b). The three functions peak around the super-solid formation. The super-cell represented in the inset of Fig. 4 (b): the blue and red balloons represent the 'A' and 'B' character, respectively. The black lines are a guide to the eye, and indicate the super-cell formation, where κ_n peaks for all n.

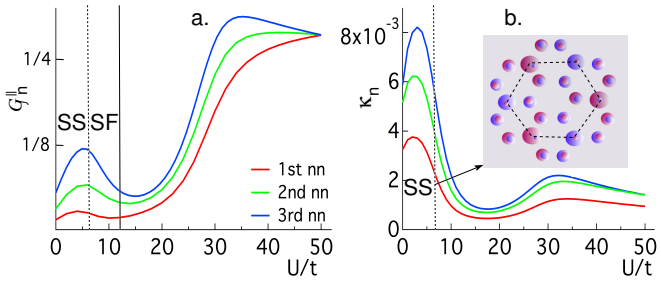

Figure 4. First (red), second (green) and third (blue) NN (a) easy-plane pair-correlation function, $\mathcal{G}^{\parallel}_n$ and (b) doubly-occupancy flip-flop pair-correlation function, κ_n. All the calculations where performed with $V = 50t$. Inset: super-solid configuration. The black broken lines mark the unit cell boundaries.

We explore further the unconventional magnetic ordering by introducing a spin-dependent lattice potential to our Hubbard Hamiltonian,

$$\widehat{V}' = \varepsilon_A \sum_{i'} \hat{n}^{i'}_{\rm A},$$

where i' indicates that the sum is performed over alternating sites (colored blue in the inset of Fig. 5). $\widehat{V}'$ leads to two sublattices, which can be experimentally implemented by employing laser beams with defined polarization [20, 21]. Introducing the symmetry breaking potential $\widehat{V}'$, the super-solid will be pinned and can be detected using easy-axis correlation functions, hence experimentally accessible. To this end, we compute the ground state of $\widehat{H} + \widehat{V}'$, for $\varepsilon_A = 0.1t$, and consider the NN population imbalance, $\langle n^i_{\rm B} - n^{i+1}_{\rm B} \rangle$. The population imbalance is expected to be maximal in the AFM regime, where the 'B' atoms would be localized in the 'i'' sublattice, decreasing towards the FM regime up to the SF regime. In the SF regime, the population imbalance should remain low and roughly constant. Fig. 5 (a) shows, however, a population imbalance peak within the SF limit (marked I). We identify this with the super-solid signal, where multiply 'B'-occupied sites appear surrounded by (dominantly) B-type NN [see inset of Fig. 4(b)]. Note that the U range for this figure differs from the previous ones, as we focus in the super-solid region. Fig 5 (b) is a slice taken at $V = 50t$, where the super-solid signal can be appreciated at nearly the same parametric regime as

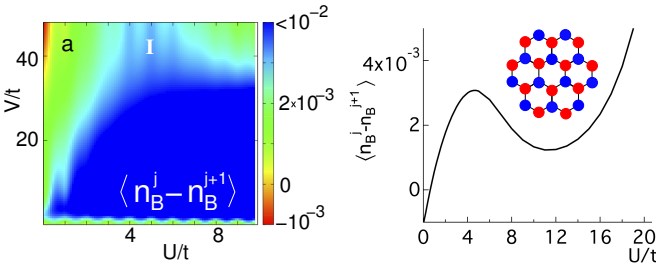

Figure 5. Expectation value of NN population difference $\langle n^i_{\rm B} - n^{i+1}_{\rm B} \rangle$ calculated for $\varepsilon_A = 0.1t$ as a function of U and V (a) and for $V = 50t$, as a function of U (b). Inset: V' defines two alternating sublattices (red and blue).

the ones for κ_n. The inset depicts the two sublattices (red and blue).

In order to account for finite size effects, we consider now a unit cell of ten sites within our hexagonal lattice structure. Fig. 6 (a) depicts the $N = 8$ FM stripe phase, whereas Fig. 6 (b) exhibits a clear domain structure indicating phase separation within the FM ordering for a $N = 10$ unit cell. We stress that $N = 10$ is not commensurate with the SS structure previously observed.

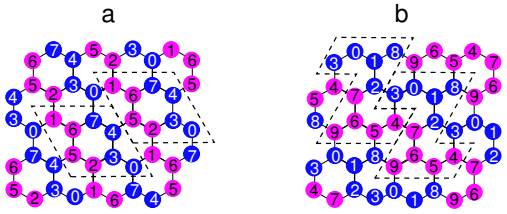

Figure 6. FM phase of (a) 8 and (b) 10 sites unit cell. The former is a stripe phase, whereas the latter presents phase separation. The broken lines depict the boundaries of two unit cells in either case.

The numerical results obtained for the ten sites unit cell where consistent with those obtained for the eight site unit cell, reproducing quite well the results presented so far. Indeed, Fig. 1 was reproduced exactly for the $N = 10$ case (not shown). Fig. 7(a) demonstrates a similar phase diagram as the one in Fig. 3 (b), where the main differences are the phase separation and the absence of SS phase, both enhancing the FM ordering (note the different color scale). Fig. 7(b) shows FM ordering in the second NN correlation, consistent with the phase separation depicted in Fig. 6 (b). We point out a small FM third NN correlations within the AFM regime in Fig. 7(c) (cyan), which appeared also in Fig. 3(c). In that region, quantum fluctuations would wash out the magnetic character, however, our normalization [40] favours the FM phase, explaining the small FM correlations. Fig. 7(c-f) shows similarities with Fig. 4(c-f), respectively, except for the absence of the super-solid signal. We would like to stress again that the absence of super-solid phase is due to the incommensurability of the super-solid periodicity with the periodic boundary conditions for the 10 sites unit cell. It is worth noting that the asymmetry of $G^{\parallel}_1$ [Fig. 7(d) and 3(d)] with respect to the $U = V$ line demonstrates a 'canted' spin phase within the

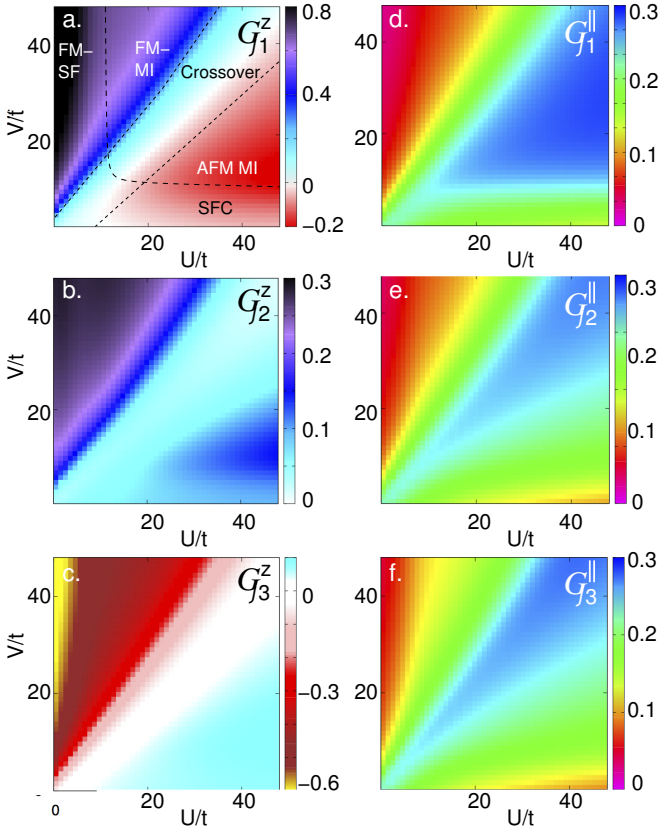

Figure 7. Numerical results for easy-axis(a-c) and easy-plane (d-e) correlation functions for first (a, d), second (b, e) and third (c, f) NN, for a 10 sites unit cell. Note the different color scales used in (a-c).

AFM regime. Note also the equivalent scales in Fig. 7(d-f) and Fig. 4(d-f), showing also large in-plane correlations in the AFM regime. These results suggest a long range FM ordering within the easy-plane component of the spin, in contrast to the short range out of plane AFM ordering.

IV. CONCLUSIONS

In summary, we calculated the extended zero-temperature quantum phase diagram of a two component Bose gas in a hexagonal lattice for MI, SF and intermediate limit. Employing an exact diagonalization method, we obtained a classification scheme based on pair correlation functions. A rich phase diagram is observed, in particular in the SF regime. Two-operator correlation functions allowed to distinguish not only between FM and AFM phases, but also between easy-axis and easy-plane ground states, bearing phase separation and SCF, respectively. Non-trivial fourth-operator correlations demonstrate the formation of a super-solid phase. Signatures of the super-solid phase could be identified in the population imbalance by artificially breaking the symmetry with a spin-dependent lattice potential, suggesting a feasible experimental method. We discriminate finite size effects by recalculating the correlations for a unit cell incommensurate with the super-solid. Easy-axis correlations for $N = 8$ and $N = 10$ sites show qualitative and quantitative resemblance, and hence, can be regarded as representative for larger systems too. Despite the small system size, the correlation functions allow us to discriminate the different phases occurring in macroscopic systems.

V. ACKNOWLEDGMENTS

We would like to thank L. Mathey, M. Potthoff, A. Chudnovskiy, and H. Niehus for valuable discussions. This work has been supported by the DFG SFB 925.

[1] Greiner, M., Mandel, O., Esslinger, T.,Hänsch, and T. W.,and Bloch, I. *Nature* **415**, 39–44 (2002).
[2] Jaksch, D., Bruder, C., Cirac, J. I., Gardiner, C. W., and Zoller, P. *Phys. Rev. Lett 81*, 3108–3111 (1998).
[3] Lewenstein, M., Sanpera, A., Ahufinger, V., Damski, B.,Sen, A., and Sen, U. *Adv. Phys.* **56**, 243–379 (2007).
[4] Bloch, I., Dalibard, J., and Zwerger, W. *Rev. Mod. Phys.* **80**, 885–964 (2008).
[5] Trotzky, S., *et al.*, *Science* **319**, 295–299 (2008).
[6] Metcalf, H. J., and van der Straten, P. Laser cooling and Trapping (Springer, Berlin, 2006).
[7] Günter, K., Stöferle, T., Moritz, H., Köhl, M., and Esslinger, T. , *Phys. Rev. Lett.* **96**, 180402 (2006)
[8] Jördens, R., Strohmaier, N., Günter, K., Moritz, H. and Esslinger, T., *Nature* **455**, 204–207 (2008).
[9] Greif, D.,Tarruell L., Uehlinger, T., Jördens, R. and Esslinger, T. *Phys. Rev. Lett.* **106**, 145302 (2011).
[10] Lühmann, D., Bongs, K., Sengstock, K. and Pfannkuche, D., *Phys. Rev. Lett.* **101**, 050402 (2008).
[11] Jo, G.B., Guzman, J., Thomas, C.K., Hosur, P., Vishwanath, A., Stamper-Kurn, D.M., *Phys. Rev. Lett.* **108**, 045305 (2012).
[12] Sachdev, S., *Phys. Rev. B* **45**, 12377 (1992).
[13] Schneider, Ch., Porras, D., and Schaetz, T., *Rep. Prog. Phys.***75** 024401 (2011).
[14] Altman, E., Hofstetter, W., Demler, E. and Lukin, M. D., *New J. Phys.* **5**, 113.1–113.19 (2003).
[15] Hubener, A., Snoek, M. and Hofstetter W., *Phys. Rev. B* **80**, 245109 (2009).
[16] Polini, M., Guinea, F., Lewenstein, M., Manoharan, H.C. Pellegrini, V., *Nat. Nano* **8** 625–633 (2013).
[17] Soltan-Panahi, P., Struck, J., Hauke, P., Bick, A., Plenkers, W., Meineke, G., Becker, C., Windpassinger, P., Lewenstein, M., and Sengstock,K., *Nat. Phys.* **7** 434–440 (2011).
[18] Uehlinger, T., Jotzu, G., Messer, M., Greif, D., Hofstetter, W., Bissbort, U., and Esslinger, T, *Phys. Rev. Lett.*, **111**, 185307 (2013).
[19] Lee, K. L., Grémaud, B., Han, R., Englert, B. G., and Miniatura, C., *Phys. Rev. A* **80**, 043411 (2009).
[20] Becker, C., Soltan-Panahi, P., Kronjäger, J., Dörscher, S. Bongs, K. and Sengstock, K., *New J. Phys.* **12** 065025 (2010).

[21] Soltan-Panahi, P., Lühmann, D.-S., Struck,J., Windpassinger P., and Klaus Sengstock, K., *Nat. Phys.* **8** 71–75 (2012).

[22] A. B. Kuklov and B. V. Svistunov, *Phys. Rev. Lett.* **90**, 100401 (2003).

[23] Duan, L.-M., Demler, E. and Lukin, M. D., *Phys. Rev. Lett.* **91**, 090402 (2003).

[24] Yang, S.-J., Lu, P., Feng, S., *Cond. Matt., arXiv:1306.5496 (2013).*

[25] He, Liang, and Li, Yongqiang, adn Ehud, Altman, and Hofstetter, W., *Phys. Rev. A* **100**, 100401 (2008).

[26] He, Liang, and Li, Yongqiang, adn Ehud, Altman, and Hofstetter, W., *Phys. Rev. A* **86**, 046320 (2012).

[27] Hu, A., Mathey, L. Danshita, I., Tiesinga, E., and Williams, C.-J., and Clark, C.-W., *Phys. Rev. A* **80**, 023619 (2009).

[28] Powell, S., *Phys. Rev. A* **79**, 053614 (2009).

[29] Endres, M., *et al.*, *Science* **334**, 200 (2011).

[30] Prokov'ev, N. *Advances in Pysics* **56**, 381–402 (2007).

[31] Kuklov, A.B., Prokof'ev,N. V. and Svistunov, B.V., Physics 4, 109 (2011).

[32] Titvinidze, I., Snoek, M. and Hofstetter, W., *Phys. Rev. Lett.* **100**, 100401 (2008).

[33] Keilmann, T., Cirac, I. and Roscilde, T. *Phys. Rev. Lett.* **102**, 255304 (2009).

[34] Hu, A., Mathey, L., Tiesinga, E., Danshita, I., Williams, C.-J., and Clark, C.-W., *Phys. Rev. A* **84**, 041609 (2011).

[35] Mathey, L. and Danshita, Ippei and Clark, Charles W., *Phys. Rev. A* **79**, 011602 (2009).

[36] Arovas, D.P., and Auerbach, A., *Phys. Rev. B* **38** 316 (1988).

[37] Zoller, P. *et al.*, Eur. Phys. J. D **36**, 203 (2005).

[38] Jaksch, D., Briegel, H. J., Cirac, J. I., Gardiner, C. W. and Zoller, P. *Phys. Rev. Lett* **82**, 1975 (1999).

[39] Mandel, O., Greiner, M., Widera, A., Rom, T., Hänsch,T. W., and Bloch, I. *Nature* **425**, 937–940 (2003).

[40] Noting that if a boson type A occupies site 'i', there are only $n_{\rm A}-1$ remaining bosons to contribute to the FM correlations whereas $n_{\rm B}$ particles may contribute to the AFM ones, we define the summ of our pair-correlation function as $\mathcal{G} = \alpha[\mathrm{FM}/(n-1) - [\mathrm{AF}]/\mathrm{n}]$, with $2n = n_{\rm A} + n_{\rm B}$ and $\alpha = (n-1/2)/(\mathrm{FM}+\mathrm{AF})$. .